In situ loading response of WC–Ni: Origins of toughness

J.W. Paggett [a],*, A.D. Krawitz [a], E.F. Drake [b], M.A.M. Bourke [c],
V. Livescu [c], B. Claussen [c], D.W. Brown [c]

[a] *University of Missouri, Columbia, MO 65211, USA*
[b] *ReedHycalog, Houston, TX 77011, USA*
[c] *Los Alamos National Laboratory, Los Alamos, NM 87545, USA*

Abstract

The strain response of WC and Ni in WC–Ni cemented carbide composites (5, 10 and 20 wt.% Ni) was studied under uniaxial compressive load to −2000 MPa using neutron diffraction. Measurements of elastic strain were made simultaneously in the axial and transverse directions of the samples, for both phases. Thermal residual stresses (TRS) were also measured, before and after loading. Ni plasticity was observed from the earliest load levels. The superposition of tensile Poisson strain (in the transverse direction) on pre-existing tensile Ni strain due to TRS produces anisotropic yielding in binder regions. Yielding is progressive with applied strain, leading to a reversal of transverse binder strain, and anisotropic relaxation of the TRS. The effect is greatest for 20 wt.% Ni, where Ni constraint is much less than for 5 wt.% Ni. These results provide a quantitative basis for the mechanical origins of the toughness of cemented carbide composites.
© 2005 Elsevier Ltd. All rights reserved.

Keywords: Cemented carbide composites; Thermal residual stress; Neutron diffraction

1. Introduction

The purpose of this study was to observe the elastic strain response of the individual phases of WC–Ni cemented carbide composites while under load. Interaction between the applied load and the thermal residual stress present in these composites due to the fabrication process is of particular interest.

A number of studies have documented the thermal residual stresses (TRS) created by the liquid phase sintering process in cemented carbide composites [1–5]. For example, the WC–20 wt.% Ni sample in the present study contains volume-averaged thermal residual stresses of about −800 MPa and +2000 MPa for the WC and Ni phases, respectively (see Table 4). The stress state

has a number of characteristics in addition to high average values [6,7]. They are the result of the difference in coefficients of thermal expansion (CTE) between the two phases, and the constraint of flow imposed by the WC particles on the Ni. Experimentally, this means that the stress state looks the same when measured in any physical direction in the samples. This is sometimes called a *diffraction hydrostatic* stress state. Furthermore, the *standard deviations* of the average values are also large [8]. In fact, the average WC compressive TRS ranges from very compressive to tensile, while the average Ni tensile TRS ranges from very tensile to compressive as observed by the broadening of diffraction peaks [1,7]. The nature of the interaction of this complex thermal residual stress state with the applied load was an important objective of this study.

The experimental method employed was stress/strain analysis using neutron diffraction [9–11]. The basic idea

---

of this method follows. A stress applied to a crystalline material creates a strain, which causes changes in interplanar spacings d. This results in changes in diffraction peak positions, through Bragg's law, $\lambda = 2d\sin\theta$, where λ is the wavelength of the radiation and θ is the angular position of the diffraction peak.

Changes in d affect θ and can, in principle, be measured to strains of 1×10^{-4}, i.e., changes as low as ± 0.0001 Å for an interplanar spacing $d = 1$ Å. Strains of the order of 1×10^{-3} are routinely measured. Note that diffraction only measures the *elastic* portion of the strain. Thus, change in *mean elastic strain* causes change in peak *positions*. The presence of strain *distributions* and/or *plastic strain* in an irradiated sampling volume causes the *shapes* of diffraction peaks to change due to variation of the interplanar spacings over the irradiated volume. This is typically seen as an increase in peak breadth [1,6,7]. Because neutrons are uncharged, they can penetrate several millimeters into WC and Ni, giving excellent bulk sampling. If multiple phases are present, they can be simultaneously and independently measured.

2. Experimental

The samples were produced and characterized by ReedHycalog (Houston, TX, USA). Three compositions were used: WC–5 wt.% Ni, WC–10 wt.% Ni, and WC–20 wt.% Ni. Metallographic properties are shown in Table 1. WC has a hexagonal structure, space group $P\bar{6}m2$, with $a = 2.9063$ Å and $c = 2.8367$ Å and Ni has a face-centered cubic structure, space group $Fm\bar{3}m$, with $a_0 = 3.5232$ Å [12]. The samples were ground and lapped to cylinders 12 mm in diameter by 28.8 mm in length, giving the sample aspect ratio (length/diameter = 2.4) required by the SMARTS instrument.

In situ measurements were made at the Los Alamos Neutron Science Center (LANSCE) [13]. LANSCE is a pulsed neutron source, which uses neutrons having a range of energies. The energies represent neutron velocities (and wavelengths) and their detection involves measuring times-of-flight of the neutrons, at fixed angles around the sample. In terms of Bragg's law, the diffraction angle θ is fixed while the wavelength λ varies. This is the inverse of the more common method used with laboratory X-rays or reactor neutron sources, for which λ is

fixed and θ varies. Time-of-flight measurements are useful for lower symmetry structures, like hexagonal WC. They enable unit cell parameters, and their changes, to be obtained from a wide range of diffraction peaks (from interplanar spacings ranging typically from 0.5 to 5 Å) using Rietveld profile refinement [14]. It is also useful for special sample environments, such as applied loads and high or low temperatures, as the spectra are collected without movement of the sample or detector.

The instrument used was the Spectrometer for MAterials Research at Temperature and Stress (SMARTS); see [15,16]. SMARTS enables compressive or tensile loads up to 250 kN to be applied to samples in situ (and, if desired, up to 1500 °C). The instrument has two banks of detectors placed 180° apart. This enables a cylindrical sample to be oriented so that diffraction data can be taken in the axial and transverse directions simultaneously. The measurement geometry is shown in Fig. 1. The count times at each load level were 7, 6, and 4 min, respectively, for the 5%, 10% and 20% Ni samples. Each WC–Ni sample was loaded and unloaded three times. The loading schedule is shown in Fig. 2.

Measurements were also made at the 10 MW University of Missouri Research Reactor (MURR). The University of Missouri Residual Stress Instrument (MURSI) [17] was used to measure the initial thermal
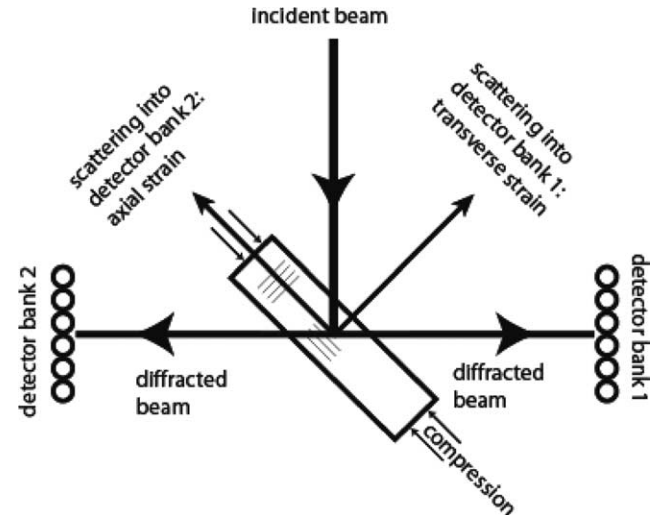

Fig. 1. Measurement geometry on SMARTS. The sample is oriented at 45° to the incident beam so that the diffraction vectors measure the axial and transverse strain in the sample simultaneously.

Table 1
Metallographic properties of WC–Ni samples

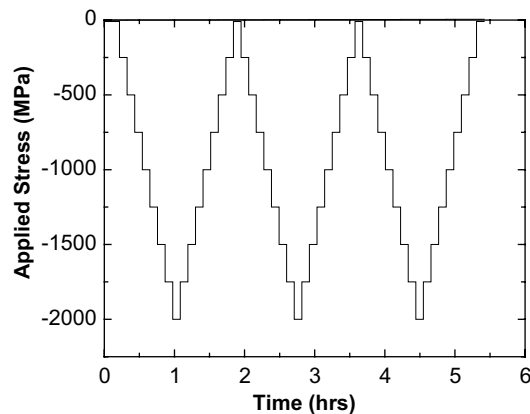| Sample (wt.% Ni)	Vol.% Ni	Density (g/cm³)	WC size (μm)	Binder mfp* (μm)	Contiguity	Hardness (rockwell A)
WC–5% Ni	7.3	15.13	1.14	0.60	0.67	90.9
WC–10% Ni	15.9	14.56	1.17	0.84	0.48	88.6
WC–20% Ni	27.6	13.68	0.93	0.80	0.45	83.9

* Mean free path.

Fig. 2. Schematic loading schedule for in situ measurements. The stress was increased in 250 MPa increments. The count time at each load level varied from 4 min (WC–5 wt.% Ni) to 7 min (WC–20 wt.% Ni).

residual stress (before sample loading) and final values after all mechanical conditioning.

3. Results and discussion

The response of the WC–5% Ni sample to the first load cycle is shown in Fig. 3. For clarity, the Ni and WC responses are separated. The Ni phase strain is calculated from the change in the lattice parameter, *a*, while the strain for the hexagonal WC phase is the average of the strain measured in the *a* and *c* directions

$$\varepsilon_{WC} = \frac{2\varepsilon_a + \varepsilon_c}{3}. \tag{1}$$

The plots show the *elastic* strain experienced by each phase as a function of applied compressive stress. Results are shown for the loading (solid symbols and solid lines) and unloading (open symbols and dashed lines) cycles, and in the axial and transverse directions. The *total composite strain* (elastic plus plastic) measured by an axial extensometer is shown on the WC figure (Fig. 3b). It shows that there is plasticity in the composite, and the Ni responses in both the axial and transverse directions (Fig. 3a) show plasticity in the Ni phase. In the transverse direction, the (elastic) Poisson Ni strain is tensile, as expected, however the accumulation of tensile strain slows and actually reverses. The WC response (Fig. 3b) is more elastic, but the WC must react to the flow of the Ni by load transfer. However, because the composite contains 93 vol.% of the much stiffer WC phase, the additional load supported by the WC is small relative to that already supported, and its effect on the applied stress–strain curve for WC is subtle. As an example, for WC–5% Ni, the difference in WC strain for a composite stress of −2000 MPa between an all-elastic and all-plastic Ni response is about 100 με, out of a total of 3000 με.
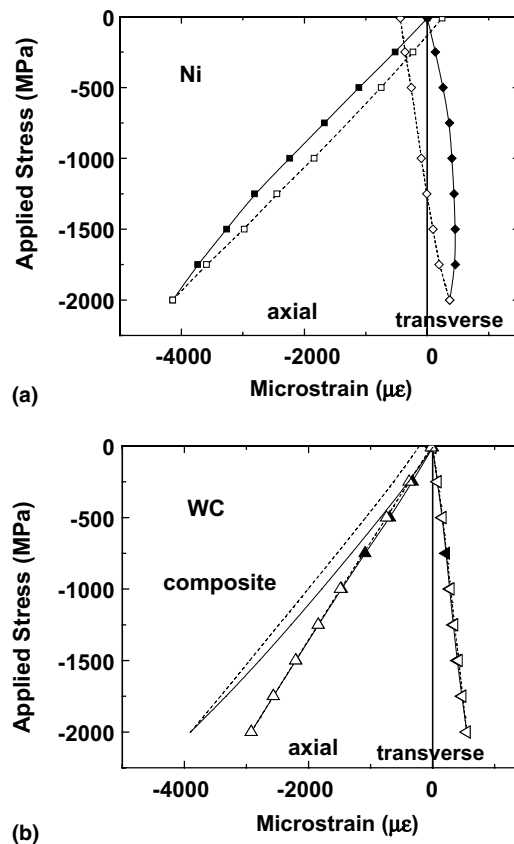

(a)

(b)

Fig. 3. WC–5 wt.% Ni. The load (solid symbols) and unload (open symbols) response of the WC and Ni phases during the first load cycle. Responses are shown in the axial and transverse directions. The WC plot also includes the composite response as measured by an axial extensometer. (It is excluded from the Ni plot because of the overlap with the axial Ni response.)

The response of the WC–20% Ni sample to the first load cycle is shown in Fig. 4. The total composite strain has a strong plastic component that is apparent from early in the loading response. As a result, the rate of increase in the axial elastic strain for the Ni slows below about −500 MPa (Fig. 4a). The most striking feature is again the transverse Ni response. As for the WC–5% Ni sample, the transverse strain initially is increasingly tensile, as expected for a compressive axial load. At about −500 MPa, however, it begins to reverse and becomes tensile at about −1200 MPa.

After unloading is complete, both compositions show hysteresis—the elastic strain does not return to its initial, unloaded value. The hysteresis is visible for both the Ni and WC phases, as well as for the macroscopic composite as measured by the extensometer. Table 2 shows the measured strain values at the end of *each* load cycle. All strain values shown are relative to the initial state of the sample after production and before loading, i.e., with the full TRS present. Although the biggest change occurs during cycle 1, the strains continue to change for cycles 2 and 3. For example, for the WC–20% Ni
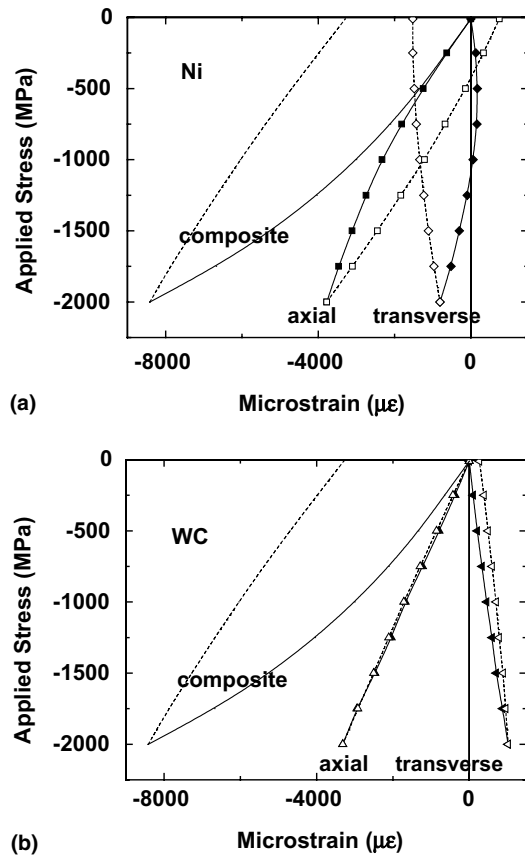
(a)

(b)

Fig. 4. WC–20 wt.% Ni. The load (solid symbols) and unload (open symbols) response of the WC and Ni phases during the first load cycle. Responses are shown in the axial and transverse directions. The composite response, as measured by an axial extensometer, is shown on both figures.

sample, the transverse Ni strain has decreased by 1523 µε at the end of cycle 1, but decreases another 110 µε during cycle 2, for a total of −1633 µε. Fig. 5 shows this effect graphically for cycles 1 and 2 of the WC–20% Ni sample. Furthermore, the data presented in Table 2 and plotted in Fig. 5 show that the relaxation is anisotropic. Although the transverse Ni strain change is negative, the axial Ni strain change is positive (Fig. 5a

and b). The plastic flow of the Ni and the constraint of the WC lead to the conversion of the *diffraction hydrostatic* stress state to a *diffraction cylindrical* stress state in the composite—a stress state that is cylindrical when averaged over the diffracting volume—for which the loading direction is the cylinder axis and the transverse directions are the cylinder radii. The axial cylindrical stress is related to the axial and transverse strains by the cylindrical expression of Hooke's Law

$$\sigma_{axial} = \frac{1}{s_2/2}\left\{\varepsilon_{axial} - \left[\frac{s_1}{s_2/2 + 3s_1}\right](2\varepsilon_{trans} + \varepsilon_{radial})\right\}, \quad (2)$$

where ε_{axial} and ε_{trans} are the axial and transverse strains, respectively, and s_1 and $s_2/2$ are the isotropic diffraction elastic constants

$$\begin{aligned} s_1 &= -\frac{v}{E} \\ s_2/2 &= \frac{1+v}{E}, \end{aligned} \quad (3)$$

where E is Young's modulus and v is Poisson's ratio. The values of s_1 and $s_2/2$ used are given in Table 3. Similarly, the transverse stress is given by

$$\sigma_{trans} = \frac{1}{s_2/2}\left\{\varepsilon_{trans} - \left[\frac{s_1}{s_2/2 + 3s_1}\right](2\varepsilon_{trans} + \varepsilon_{axial})\right\}. \quad (4)$$

Table 4 shows the measured residual stresses in the as-produced samples and after all loading cycles. Initial thermal residual stresses were derived from measuring the shift in position of the WC 201 peak between as-produced samples and a WC powder reference. The strain was calculated from the peak positions by

$$\varepsilon = \frac{\sin\theta_0}{\sin\theta} - 1, \quad (5)$$

where θ_0 is the position of the reference powder peak and θ is the position of the peak in the as-produced sample. The thermal residual stress was then calculated from Hooke's Law, i.e.,

$$\sigma = \frac{E}{1-2v}\varepsilon, \quad (6)$$

Table 2
Residual strain values after each load–unload cycle

Sample	Cycle	Macro (µε)	Axial (µε)		Transverse (µε)	
			WC	Ni	WC	Ni
5 wt.% Ni	1	−231 ± 24	−23 ± 18	242 ± 44	−4 ± 13	−439 ± 28
	2	−242 ± 23	−8 ± 18	343 ± 44	−2 ± 13	−504 ± 28
	3	−250 ± 23	−44 ± 18	354 ± 44	−2 ± 13	−568 ± 28
20 wt.% Ni	1	−3292 ± 23	3 ± 32	748 ± 17	268 ± 25	−1523 ± 15
	2	−3521 ± 24	−20 ± 32	836 ± 17	282 ± 25	−1633 ± 15
	3	−3640 ± 25	25 ± 32	872 ± 18	296 ± 25	−1685 ± 15

All values are relative to the initial unloaded samples, which have the as-produced TRS values shown in Table 2. Macroscopic composite values are determined from the extensometer and are the total (elastic plus plastic) residual strains; WC and Ni values are determined from diffraction, and are elastic.
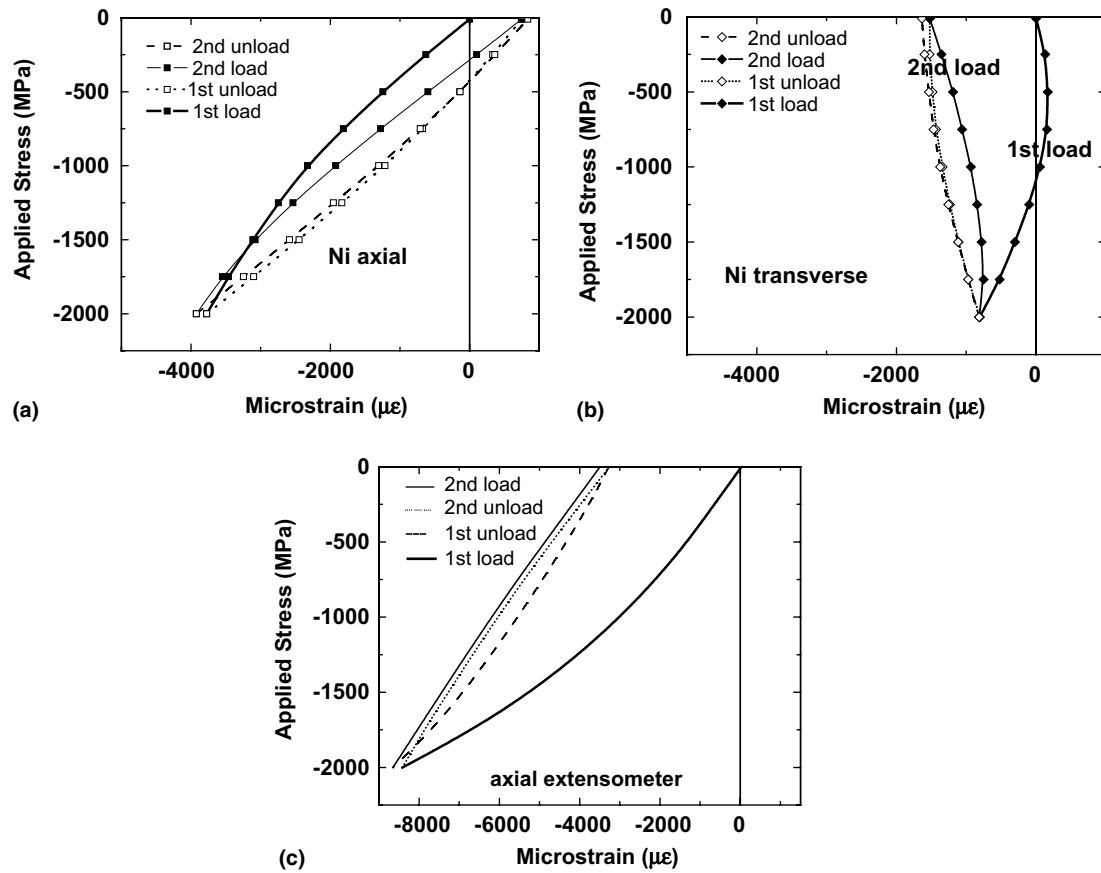
Fig. 5. WC–20 wt.% Ni. The first two load–unload cycles. The plots are broken into three parts: the nickel axial direction; the Ni transverse direction; and, the macroscopic (elastic plus plastic) extensometer response. The scales have been expanded for the Ni axial and transverse plots.

Table 3
Diffraction elastic constants for cylindrical stress calculations

Phase	s_1 (MPa^{-1} × 10^{-6})	$s_2/2$ (MPa^{-1} × 10^{-6})
Ni	−1.9559	7.6726
WC	−0.3539	1.8214

Values for the Ni phase are based on [18] and the values for the WC phase are averages of the (100), (010), and (001) directions using values based on [1].

Table 4
Residual stress measurements for WC–Ni samples in the as-produced condition, and after all loading cycles

Sample	Phase	As-produced (MPa)	After loading	
			Axial (MPa)	Transverse (MPa)
WC–5% Ni	WC	−231 ± 43	−256 ± 47	−227 ± 55
	Ni	2940 ± 256	2931 ± 599	2798 ± 600
WC–20% Ni	WC	−764 ± 88	−614 ± 91	−422 ± 90
	Ni	2005 ± 207	1855 ± 168	1460 ± 168

All data taken on MURSI.

where E is Young's modulus and v is Poisson's ratio. The elastic constants used for these measurements are the values for the WC 201 lattice planes, $E = 692$ GPa and $v = 0.25$ derived from [1]. The thermal residual stress in the Ni phase of the as-produced samples were calculated from a force balance with the WC phase from

$$(1 - f)\sigma_{WC} + f\sigma_{Ni} = 0, \tag{7}$$

where f is the volume fraction of Ni in the sample, σ_{WC} is the measured stress in the WC phase, and σ_{Ni} is the calculated stress in the Ni phase. The change in residual stress between the as-produced and mechanically loaded samples was found by measuring the shift in peak position (WC 201 and Ni 311 peaks). The changes in stress were then calculated from Eq. (5) and Eqs. (2) and (3). These changes in residual stress were then added to the initial TRS to obtain the total residual stress after mechanical loading.

Table 4 shows that the Ni residual stress has been reduced in both the axial and transverse directions, but by different amounts. For example, the Ni phase in the WC–20% Ni sample starts with a volume-averaged diffraction hydrostatic TRS of +2005 MPa in all directions in the sample. After the loading cycles, it reduces by 150 MPa to +1855 MPa in the axial direction and by 545 MPa to +1460 MPa in the transverse direction.
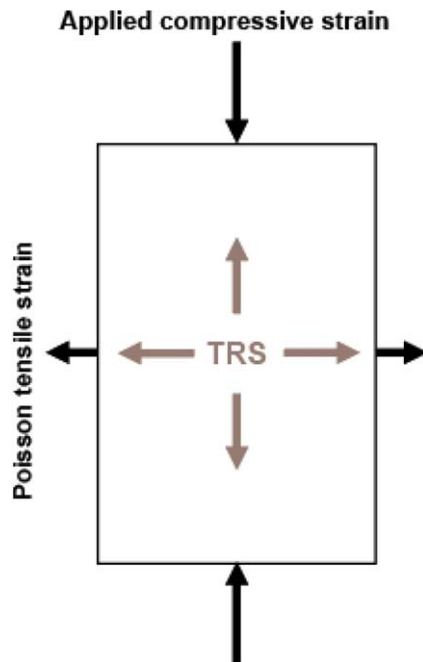
Applied compressive strain

Fig. 6. Relation between the thermal residual strain in the Ni (grey) and the applied compressive strain (black).

Such anisotropic stress relaxation has been previously observed [19]. The response is related to the interaction of the applied stress and the pre-existing TRS. The binder is under an average tensile residual stress. Upon application of a compressive axial stress, a compressive axial strain and a tensile radial (Poisson) strain interact with the average tensile TRS; see Fig. 6. This leads to local plastic flow in the binder that is greater in the transverse (Poisson) direction than in the axial direction because the critical shear stress is exceeded. Local shear can occur more readily in the transverse direction because the imposed radial tensile strain adds to the pre-existing tensile strain, which is locally very high. In the axial direction, the response is more elastic because the applied compressive strain acts to lower the tensile TRS. Although the TRS distribution extends locally into compression, the magnitudes are not nearly as high as the tensile regions. Thus, most of the flow is expected in tensile regions. The measured reduction in residual stress can, in principle, occur not only by relaxation of the TRS in the Ni but also by the creation of mechanically induced residual stresses opposite in sign to the TRS due to differential flow of the Ni relative to the WC. Since these are residual micro-stresses on a fine microstructural scale, localized tensile flow in the Ni at locations throughout the microstructure seems more likely. Thus, some of the transverse tensile elastic TRS in the Ni converts to plastic stress, initiating relaxation in the axial direction in the Ni. This in turn requires a counterbalancing relaxation in the WC that would be smaller in magnitude than for the Ni due to the greater amount of WC in the material.

Finally, it is noted that a finite element analysis of companion WC–Co samples has been performed and is discussed in Ref. [20]. It provides a good prediction of the neutron results for low Co content, i.e., for more constrained, elastic systems.

4. Conclusions

The mechanical response of WC–Ni cemented carbide composites to uniaxial compression reflects characteristic complex non-linear behavior that results from aggregate micro-scale yielding and relaxation. The composites exhibit bulk plasticity at all load levels. This plasticity arises from interaction of the applied load with pre-existing thermal residual stresses. Since discrete binder regions throughout the composite are pre-stressed to the critical resolved shear stress threshold, every applied strain increment triggers local plastic strain in those critical regions oriented such that the applied shear vector is additive. In compressive loading, these events predominate in the transverse direction where tensile Poisson response is additive to the tensile binder TRS bias, producing pronounced anisotropy. A study of the nature of strain/stress distributions in cemented carbide composites [7] indicated that the stress distributions in cemented carbides are primarily due to variations of the deviatoric component of the stress tensor at each point. That is, there are two limiting cases for the stress distribution: (1) point to point variation of the hydrostatic component, and (2) variation with angle of the deviatoric component at each point. This implies that those locations with high shear components in the transverse direction would be the most likely to flow.

The observation that discrete micro-scale yield events aggregate to cause characteristic macroscale plasticity behavior at all strain levels is significant for the understanding of toughness behavior. The non-conservative plastic part of the bulk strain response corresponds to strain energy absorption, which is the primary toughening mechanism in metals. Since toughness of ductile materials is usually modeled as the stability of a crack defect in terms of elastic and plastic zones within a strained continuum, the peculiar stress–strain behavior of cemented carbides means that their fracture mechanics treatment should require that the plastic zone equal the component dimensions. Or in other words, the character of the stress field produced by external loading of a cemented carbide component is affected throughout by both plastic and elastic response at all load increments. The additional fact that plastic absorption of applied elastic strain energy also causes cancellation and redistribution of internal residual elastic strains provides an independent (and complicating) influence on the character of the applied stress field. These effects remain to be quantified in terms of their influence on the toughness

we measure, but it is intuitive that they are the source of the toughness anomaly exploited in this composite family.

Acknowledgements

References

[1] Krawitz AD, Reichel DG, Hitterman RL. Residual stress and stress distribution in a WC–Ni composite. Mater Sci Eng 1989;A119:127–34.

[2] Krawitz AD, Roberts R, Faber J. Residual stress relaxation in cemented carbide composites. In: Science of Hard Materials, Inst of Physics Conf Series No. 1; 1986. p. 577–89.

[3] Majumdar S, Singh JP, Kupperman D, Krawitz AD. Application of neutron diffraction to measure residual strains in various engineering composite materials. ASME J Eng Mater Technol 1991;113:51–9.

[4] Mari D, Krawitz AD, Richardson JW, Benoit W. Residual stress in WC–Co measured by neutron diffraction. Mater Sci Eng 1996;A209:197–205.

[5] Coats DL, Krawitz AD. Effect of particle size on thermal residual stress in WC–Co composites. Mater Sci Eng 2003;A359:338–42.

[6] Weisbrook CM, Gopalaratnam VS, Krawitz AD. Use of finite element modeling to interpret diffraction peak broadening from elastic strain distributions. Mater Sci Eng 1995;A201:134–42.

[7] Weisbrook CM, Krawitz AD. Thermal residual stress distribution in WC–Ni composites. Mater Sci Eng 1996;A209:318–28.

[8] Krawitz AD, Winholtz RA, Weisbrook CM. Relation of elastic strain distributions determined by diffraction to corresponding stress distributions. Mater Sci Eng 1996;A206:176–82.

[9] Krawitz AD. Introduction to diffraction in materials science and engineering. New York: John Wiley & Sons; 2001.

[10] Noyan IC, Cohen JB. Residual stress: measurement by diffraction and interpretation. New York: Springer-Verlag; 1987.

[11] Krawitz AD. Stress measurements in composites using neutrons. In: Hutchings MT, Krawitz AD, editors. The measurement of residual and applied stress using neutron diffraction. New York: Kluwer Academic Pubs; 1992. p. 405–20.

[12] Villars P, Calvert LD. Pearson's handbook of crystallographic data for intermetallic phases. Materials Park, OH: American Society of Metals; 1985.

[13] Los Alamos Neutron Scattering Science Center, Available from: <http://lansce.lanl.gov/>.

[14] Rietveld HM. A profile refinement method for nuclear and magnetic structures. J Appl Cryst 1969;2:65–71.

[15] SMARTS, Available from: <http://lansce.lanl.gov/lujan/ER1ER2/SMARTs/index.html>.

[16] Bourke M, Dunand D, Ustundag E. SMARTS—a spectrometer for strain measurement in engineering materials. Appl Phys A: Mater Sci Process 2002;A74:S1707.

[17] Witte DA, Krawitz AD, Winholtz RA, Berliner RR, Popovici M. An instrument for stress measurement using neutron diffraction. J Neutron Res 1998;6:217–32.

[18] Hearmon RFS. The elastic constants of anisotropic materials II. Adv Phys 1956;5:323–82.

[19] Seol K, Krawitz AD. Anisotropic residual stress relaxation in cemented carbide composites. Mater Sci Eng 1990;A127:1–5.

[20] Livescu V, Clausen B, Paggett JW, Krawitz AD, Drake EF, Bourke MAM. Measurement and modeling of room temperature co-deformation in WC–10 wt.% Co. Mater Sci Eng A, in press.